Degeneration of Neural Cells in the Central Nervous System of Mice Deficient in the Gene for the Adhesion Molecule on Glia, the β2 Subunit of Murine Na,K-ATPase

Josef Peter Magyar, Udo Bartsch, Zhao-Qi Wang,* Norma Howells,* Adriano Aguzzi,* Erwin F. Wagner,* and Melitta Schachner

Department of Neurobiology, Swiss Federal Institute of Technology, Hönggerberg, CH-8093 Zurich, Switzerland; and *Institute of Molecular Pathology, A-1030 Vienna, Austria

Abstract. We generated mice, null mutant in the adhesion molecule on glia (AMOG), the β2 subunit of the murine Na,K-ATPase gene. These mice exhibit motor incoordination at 15 d of age, subsequently tremor and paralysis of extremities, and die at 17–18 d after birth. At these ages, the mutants have enlarged ventricles, degenerating photoreceptor cells, and swelling and degeneration of astrocytic endfeet, leading to vacuoles adjoining capillaries of brain stem, thalamus, striatum, and spinal cord. In tissue homogenates from entire brains of 16–17-d-old mutants, Na,K-ATPase activity and expression of the β1 subunit of the Na,K-ATPase and of the neural adhesion molecules L1, N-CAM, and MAG appear normal. We suggest that the mutant phenotype can be related primarily to reduced pump activity, with neural degeneration as a possible consequence of osmotic imbalance.

THE adhesion molecule on glia (AMOG)[1] was first described as a Ca^{2+}-independent murine recognition molecule that mediates neuron-to-astrocyte interaction in vitro and that is functionally involved in the migration of granule cells along Bergmann glial fibers in cerebellar explant cultures (Antonicek et al., 1987). Subsequently, AMOG has been termed AMOG/β2, since sequence analysis revealed AMOG to be a close homologue of the β1 subunit of the Na,K-ATPase (Gloor et al., 1990). A β2 subunit of the Na,K-ATPase was also identified in rats and humans by low stringency hybridization using a β1 subunit probe (Martin-Vasello et al., 1989).

The Na,K-ATPase is a membrane-bound ion pump consisting of one catalytic α (α1, α2 or α3) subunit and one β (β1 or β2) subunit, the function of which has not yet clearly been established. AMOG/β2 is tightly associated with the α subunit of the Na,K-ATPase, since α2, to a lesser extent, also α3 copurifies with AMOG/β2 during stringent immunoaffinity chromatography isolation procedures from adult mouse brain (Gloor et al., 1990). Furthermore, expression of AMOG/β2 in *Xenopus laevis* oocytes in the presence of endogenous or coexpressed α subunits reconstitutes a functional Na,K-ATPase (Schmalzing et al., 1992). Last, a monoclonal antibody to AMOG/β2 that blocks adhesion, triggers Na,K-ATPase-specific Rb^+ uptake of cultured astrocytes by its ability to increase pump activity (Gloor et al., 1990).

AMOG/β2, which carries the oligomannosidic L3 carbohydrate structure (Schmitz et al., 1993) expressed also by other neural recognition molecules (Kücherer et al., 1987; Fahrig et al., 1990; Bollensen and Schachner, 1987; Pesheva et al., 1987; Horstkorte et al., 1993), has also been characterized as a recognition molecule by several operational criteria. Liposomes containing immunoaffinity purified AMOG/β2 bind specifically to cell surfaces of distinct neuronal cell types (Antonicek and Schachner, 1988). Furthermore, elimination of pump activity during the adhesion assay either with ouabain or by reducing the temperature to 4°C does not abolish AMOG/β2-dependent neuron-to-astrocyte adhesion (Gloor et al., 1990). Finally, expression of AMOG/β2, but not that of β1 subunit of the Na,K-ATPase on the cell surface of fibroblasts, enhances neurite outgrowth of cocultured small cerebellar neurons (Müller-Husmann et al., 1993). Monoclonal AMOG/β2 antibodies or recombinantly expressed AMOG/β2 protein inhibit this increase in neurite

J. P. Magyar and U. Bartsch contributed equally to this work.

Address all correspondence to Dr. Melitta Schachner, Department of Neurobiology, Swiss Federal Institute of Technology, Hönggerberg, CH-8093 Zürich, Switzerland. Telephone: 41-1-633-3396; FAX: 41-1-633-1046.

The present address of Dr. J. P. Magyar is Institute of Cell Biology, Swiss Federal Institute of Technology, Hönggerberg, CH-8093 Zurich, Switzerland.

The present address of Dr. A. Aguzzi is Institute of Neuropathology, University of Zürich, Schmelzbergstrasse, CH-8091 Zürich, Switzerland.

1. *Abbreviations used in this paper*: AMOG, adhesion molecule on glia; AMOG/β2, adhesion molecule on glia, the β2 subunit of the Na,K-ATPase; AMOG $^{(0/0)}$, homozygous AMOG deficient; AMOG$^{(+/0)}$, heterozygous AMOG deficient; AMOG $^{(+/+)}$, wild type.

outgrowth on AMOG/β2 transfected fibroblasts, but not on nontransfected fibroblasts or on fibroblasts transfected with the β1 subunit (Müller-Husmann et al., 1993).

The characterization of AMOG/β2 as a cell recognition molecule and as a subunit of the Na,K-ATPase introduces a new concept in the link between cell recognition and signal transduction: coupling of cell recognition with ion transport implicates cell–cell interactions in the regulation of the ionic milieu. Concentrations of both Na^+ and K^+ determine the membrane potential of cells and thus activity of voltage-dependent ion channels (Hodgkin, 1964; Hille, 1984), size of extracellular space, and thus also cell volume (Kimelberg, 1991). Persistence of AMOG/β2 expression in the adult, particularly in cerebellum and hippocampus (Pagliusi et al., 1990), suggests that cell contacts between neurons and astrocytes may be instrumental in regulating the ionic symbiosis between neural cells.

To analyze how the two functions of AMOG/β2 are combined to influence development and maintenance of nervous tissue, we have generated a mouse deficient in the expression of the AMOG/β2 gene (Magyar and Schachner, 1990). Here we show that the null mutation in the AMOG/β2 gene affects the morphological integrity of several, but not all neural cell types which express AMOG/β2. We suggest that most of the histological abnormalities observed shortly before the mutant's death result from alterations of ionic homeostasis.

Materials and Methods

AMOG/β2 Gene Targeting and PCR Mock Construct

A mutation was inserted into the first exon of the AMOG/β2 genomic clone G7SH (Magyar and Schachner, 1990) by subcloning the PvuII fragment of G7SH into the PvuII site of vector pSP72 (Promega, Madison, WI). An oligonucleotide (5'-TATGACTCGAGCTAGCGTAGC-3' hybridized with 5'-TACGCTAGCTCGAGTCATAGC-3') was inserted into the SacII site of this fragment generating a unique XhoI site and two in frame stop codons. After reintroduction of this mutated PvuII fragment into G7SH, the XhoI-SalI neo^r cassette from pMC1neo Poly A (Stratagene, La Jolla, CA) was subcloned into the XhoI site and designated G7SHneo. The neo^r cassette was in the same transcriptional orientation as the AMOG/β2 gene. The 5' arm of G7SHneo was shortened to 1 kb by digestion with HindIII and SnaBI followed by religation. The resulting construct was designated AMOGneo. The XhoI–SalI fragment of pIC19R/MC-1-tk (Mansour et al., 1988) containing the HSV-tk cassette was then inserted into the SacII site of AMOGneo and designated AMOGtk. NotI linearized AMOGtk was used for electroporation of embryonic stem cells. To construct a mock vector for PCR screening, the G7SHneo was linearized with HindIII and used for optimization and control of the PCR reaction.

Growth, Transfection, and Selectin of Embryonic Stem Cells

Culture, transfection with NotI linearized AMOGtk, and double selection of the embryonic stem cell line D3 (Doetschman et al., 1985) was carried out as described (Soriano et al., 1991; Giese et al., 1992).

PCR Screening of Recombinant Clones and Southern Blot Analysis

Picking of G418 and FIAU (1-[2-deoxy,2-fluoro-β-D-arabinofuranosyl]-5-iodouracyl) resistant clones and lysis of pools were performed as described previously (Soriano et al., 1991). Half of the lysate was amplified in a final volume of 25 μl in 1 × PCR buffer (16.6 mM $(NH_4)_2SO_4$, 67 mM Tris-HCl (pH 8.8), 6.7 mM $MgCl_2$, 5 mM 2-mercaptoethanol, and 6.7 μM ethylenediaminetetraacetic acid; Kogan et al., 1987), 1 mM each 2'-deoxynucleotide-5'-triphosphate (Pharmacia LKB Biotechnology, Piscataway, NJ), 120 nM primer each, 10% dimethyl sulfoxide, 80 μg/ml BSA and 25 U/ml Taq DNA polymerase (Perkin Elmer Cetus, Norwalk, CT). Amplifications were carried out for 40 cycles of 30 s at 93°C, 30 s at 56°C, and 2 min at 65°C. Primers for the reaction were derived from AMOG/β2 genomic sequences upstream of the targeting vector homologous region (5'-TCACATTCAGCCCTCTGTTC-3') and from the neo cassette (5'-TGC-AAAACCACACTGCTCGA-3').

PCR conditions were established from amplifications of dilution series of the PCR construct (G7SHneo) in the presence or absence of 300 ng mouse genomic DNA per reaction. Under the conditions used, the amplification product of 1 fg template was detectable on an ethidium bromide–stained agarose gel.

For Southern blot analysis, 5–10 μg genomic DNA from the PCR-positive clones or from mouse tail biopsies was digested with BamHI or EcoRI. Obtained fragments were separated on an agarose gel and transferred with 0.4 M NaOH to Hybond N^+ membrane (Amersham Corp., Arlington Heights, IL). Hybridization probes were labeled by random priming to a specific activity of at least 10^9 cpm/μg DNA. As probes, the 5'-external probe (416 bp StyI-SnaBI fragment of the AMOG/β2 gene lying upstream of the construct) or the neo^r cassette were used. Hybridization, washing, and stripping conditions were according to the manufacturer's recommendations.

Blastocyst Injections and Mating of Chimeric Mice

C57BL/6J blastocysts were injected with AMOG/β2-targeted ES cells as described previously (Wang et al., 1991). Male chimeras were mated with C57BL/6J females. The heterozygous offspring were paired to obtain homozygous mice. Genotypes of mice were determined by Southern blot analysis using the 5'-external probe.

Determination of Na,K-ATPase Activity

The Na,K-ATPase activity was determined by the timed test tube assay according to Müller-Husmann et al. (1993).

Antibodies

Production and purification of polyclonal rabbit antibodies to immunoaffinity purified L1 (Rathjen and Schachner, 1984), N-CAM (Keilhauer et al., 1985), MAG (Poltorak et al., 1987), and to the β1 subunit of the Na,K-ATPase (Schmalzing et al., 1991) have been described. Polyclonal antibodies against L1 and N-CAM were immunoaffinity purified on L1 and N-CAM coupled to Sepharose 4B (Martini and Schachner, 1986). Additionally, polyclonal rabbit AMOG/β2 antibodies (Antonicek et al., 1987), the rat monoclonal AMOG/β2 antibodies 426, 614 (prepared according to Antonicek et al., 1987) and B8 (Schmidt, C., personal communication), the mouse monoclonal antibody gp 50 (Beesley et al., 1987) reacting with AMOG/β2 (Gloor, S., and G. Müller-Husmann, personal communication), and the monoclonal rat antibody BSP-3 (Gorvel et al., 1984) specific for the β1 subunit of the Na,KATPase were used.

For Western blot analysis, polyclonal and monoclonal antibodies were visualized by horseradish peroxidase–conjugated antibodies to mouse IgG and IgM, to rat IgG and to rabbit IgG (all from Dianova, Hamburg, Germany). For immunocytochemistry, primary antibodies were detected using fluorescein isothiocyanate–conjugated goat anti-rat antibodies (Dianova). Digoxigenin-labeled cRNA probes for in situ hybridization were visualized by alkaline phosphatase–conjugated Fab fragments to digoxigenin (Boehringer Mannheim Corp., Indianapolis, IN).

Western Blot Analysis

Brains from 16 to 18-d-old mice were homogenized with a Dounce homogenizer in homogenization buffer (50 mM Na_2HPO_4, 100 mM NaCl, 0.2 mM $MgCl_2$, 0.2 mM $CaCl_2$, 1 mM spermidine). After sonification, membranes were isolated by centrifugation and washed two times with homogenization buffer (Antonicek et al., 1987). The protein content was determined (according to Bradford, 1976). Proteins (200 μg) were analyzed by Western blotting under nonreducing conditions using the polyclonal antibodies to AMOG/β2 (dilution 1:500), to L1 (dilution 1:2,000), to N-CAM (dilution 1:5,000), to MAG (dilution 1:10,000), and to the β1 subunit of Na,K-ATPase (10 μg/ml) or using the AMOG/β2 monoclonal antibodies 614 (dilution 1:1,000), 426 (dilution 1:500), gp 50 (dilution 1:500), and B8 (dilution 1:500). Horseradish peroxidase–conjugated secondary antibodies (dilution 1:1,000) were detected by ECL (Amersham, Buckinghamshire, GB).

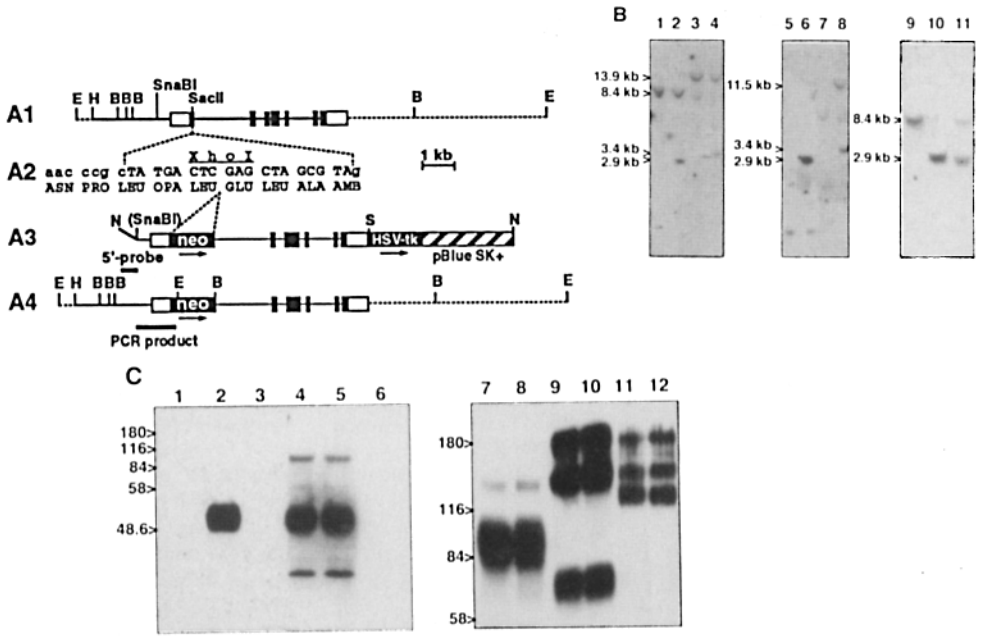

Figure 1. (*A1*) AMOG/β2 gene, (*A3*) AMOG/β2 gene-targeting construct, and (*A4*) the mutated AMOG/β2 gene, (*B*) verification of the replacement of the AMOG/β2 gene by the AMOG/β2 gene-targeting construct by Southern blot analysis and (*C*) Western blot analysis of the expression of the β subunits of the Na,K-ATPase and several recognition molecules in crude brain membrane preparations. (*A1*) Restriction map of the AMOG/β2 gene according to Magyar and Schachner (1991). Closed boxes represent the coding regions of exons. Relevant restriction sites are abbreviated as follows: *B*, BamHI; *E*, EcoRI; *H*, HindIII; *S*, SalI. (*A2*) An oligonucleotide (indicated in capital characters, sequence beginning with amino acid 23; Gloor et al., 1990) was inserted into the first exon of the AMOG/β2 gene to generate 2 in frame stop codons and a new and unique XhoI restriction endonuclease site. (*A3*) Restriction map of the AMOG/β2 gene-targeting construct, AMOGtk, containing homologous sequences of 1 kb on the 5′ and 4.7 kb on the 3′ side of the neo insertion. Transcriptional orientation of the neo and HSV-tk genes is indicated by arrows. *N* represents a cleavage site for NotI originating from the cloning site of the vector. (*A4*) Observed S1 and L1 replacement event of the AMOG/β2 gene (for nomenclature see Hasty et al., 1991). In such an event, the indicated PCR product will be formed. (*B*) Southern blot analysis of DNA samples from ES cells (lanes *1*, *3*, *5*, and *7 not targeted*; lanes *2*, *4*, *6*, and *8 targeted*) and from AMOG$^{(+/+)}$ (lane *9*), AMOG$^{(0/0)}$ (lane *10*), and AMOG$^{(+/0)}$ (lane *11*) mouse tail biopsies. The DNA was digested either with BamHI (lanes *1*, *2*, *5*, *6*, and *9–11*) or with EcoRI (lanes *3*, *4*, *7*, and *8*) and was hybridized either with the 5′-external probe (lanes *1–4* and *9–11*) or with the neo probe (lanes *5–8*). (*C*) Western blot analysis of crude membrane fractions of brains from 18-d-old AMOG$^{(0/0)}$ (*lanes with odd numbers*) and AMOG$^{(+/+)}$ (*lanes with even numbers*) mice. The blot was developed with a monoclonal AMOG/β2 antibody (lanes *2* and *3*), polyclonal antibodies to the β1 subunit of the Na,K-ATPase (lanes *4* and *5*), and with polyclonal antibodies directed against MAG (lanes *7* and *8*) L1 (lanes *9* and *10*), and N-CAM (lanes *11* and *12*). Lanes *1* and *6* are controls in which first antibodies were omitted for lanes *2–3* and *4–5*, respectively.

Light and Electron Microscopy

For light and electron microscopy, animals were deeply anaesthetized and perfused through the left ventricle with 4% paraformaldehyde and 2% glutaraldehyde in phosphate buffer (pH 7.4). Tissue was removed and postfixed in the same fixative. Eyes were fixed by immersion in 2% paraformaldehyde and 2% glutaraldehyde in 0.1 M cacodylate buffer (pH 7.4). Vibratome sections, 100–200 μm in thickness, were incubated in 1% OsO_4 for 30 min, dehydrated in an ascending series of acetone and embedded in Spurr's epoxy resin. For light microscopy, 1-3-μm thick sections were stained with Toluidine blue and examined with a Zeiss Axiophot. For electron microscopy, ultrathin sections were counterstained with uranyl acetate and lead citrate and examined with a Zeiss EM 10.

Indirect Light Microscopic Immunocytochemistry

For indirect light microscopic immunocytochemistry, eyes, optic nerves, and cerebella were removed, embedded in O.C.T. (Miles, Elkhart, IN), and frozen in liquid nitrogen-cooled 2-methylbutane. Cryostat sections, 14 μm in thickness, were thaw-mounted onto poly-L-lysine-coated coverslips and air-dried. Immunocytochemistry was performed as described elsewhere (Bartsch et al., 1989; Bartsch et al., 1992*a*).

In Situ Hybridization

In situ hybridization analysis of tissue sections from cerebella, retinae, and optic nerves was carried out as described in detail elsewhere (Bartsch et al., 1992*a*,*b*). Since the non-radioactive digoxigenin-based immunocytochemical detection of hybridized cRNA is as sensitive as radioactive-labeling technique (Dörries et al., 1993) and produces less background labeling, even low levels of mRNA could be unequivocally detected (for comparison see Pagliusi et al., 1990).

The 625-bp ApaI–SacII fragment of the AMOG/β2 genomic clone G7SH (Magyar and Schachner, 1990), encompassing the region of the first exon of AMOG/β2 situated upstream of the mutation in the AMOG gene, was subcloned into the ApaI–SacII site of BluescriptKS+ and BluescriptSK+. These plasmids were linearized with SacII and ApaI, respectively, and used for transcription with T3-DNA polymerase to produce digoxigenin-labeled riboprobes (Bartsch et al., 1992*a*; Dörres et al., 1993).

The 548-bp HindIII–SnaBI fragment of the Na,K-ATPase β1 subunit cDNA (Gloor, 1989), encoding the COOH-terminal part and 91 bp noncoding sequence of the β1 subunit, was subcloned into the HindIII–SmaI site of BluescriptKS+ and BluescriptSK+. These plasmids were linearized with BamHI or HindIII, respectively, and used for transcription with the T3-DNA polymerase.

Results

Generation of AMOG$^{(0/0)}$ Mice

The AMOG/β2-targeting construct AMOGtk (Fig. 1 *A*) includes 5.5 kb of homologous sequence and a neo gene expression cassette inserted in the first coding exon of the AMOG/β2 gene in the same transcriptional orientation as AMOG/β2. Since alternative splice sites in the AMOG/β2 gene have not been observed (Magyar and Schachner, 1990; Shyjan et al., 1991), replacement of the endogenous gene by

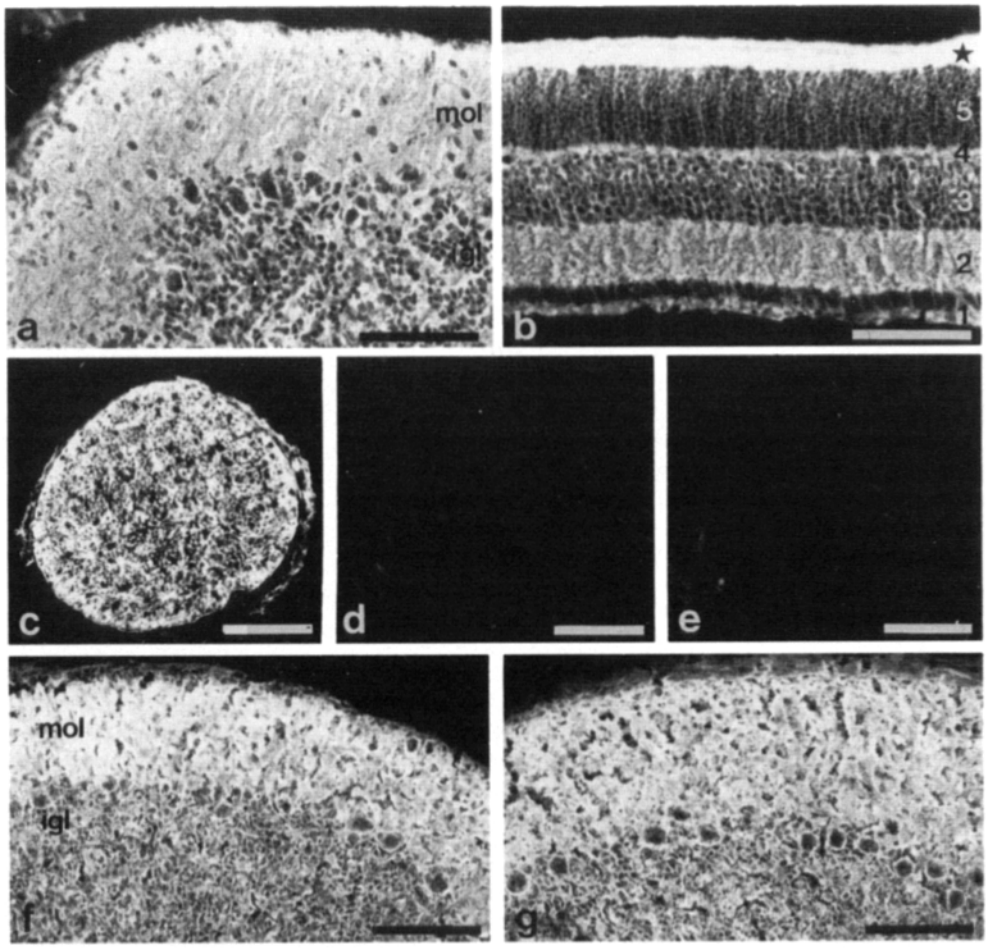

Figure 2. Immunocytochemical localization of AMOG/β2 (*a–c*, *e*) and β1 (*f* and *g*) in the cerebellar cortex (*a*, *f*, and *g*), retina (*b*), and optic nerve (*c* and *e*) of 17-d-old AMOG$^{(+/+)}$ (*a–c*, and *f*) and AMOG$^{(0/0)}$ (*e* and *g*) littermates using monoclonal antibodies. AMOG/β2 is strongly expressed in the molecular layer (*mol*) and internal granular layer (*igl*; *a*). In the retina, AMOG/β2 immunoreactivity is detectable in the nerve fiber layer (*1*), the inner (*2*) and outer (*4*) plexiform layers, and the inner (*3*) and outer (*5*) nuclear layers (*b*). Strongest immunoreactivity is detectable between the apical border of the outer nuclear layer and the outer segments of photoreceptor cells (*asterisk in b*). In the myelinated part of the optic nerve, AMOG/β2 immunolabeling is homogeneously distributed (*c*). Sections from optic nerves of AMOG$^{(+/+)}$ animals which were incubated with secondary antibodies only (*d*) showed a weak background labeling similar to that observed in sections from AMOG$^{(0/0)}$ littermates (*e*) incubated with primary and secondary antibodies. In the cerebellar cortex β1 is homogeneously distributed in the molecular layer (*mol*) and internal granular layer (*igl*) with a similar intensity in expression in AMOG$^{(+/+)}$ (*f*) and AMOG$^{(0/0)}$ (*g*) animals. Bars: (*a–g*) 100 μm.

the gene-targeting construct AMOGtk should result in a null mutation.

Linearized AMOGtk was electroporated into D3 embryonic stem cells, and seven potential recombinants were identified by PCR among 184 clones resistant to both G418 and FIAU. Targeted integration into the AMOG/β2 gene (Fig. 1 *A*) was verified by Southern blot analysis using a hybridization probe located 5′ upstream to the targeting construct (Fig. 1 *B*; lanes *1–4*). The endogenous 8.4-kb BamHI and 13.9-kb EcoRI fragments were found to be reduced to 2.9 and 3.4 kb, respectively, as expected for homologous recombination of the short 5′-arm of AMOGtk. Using the neo cassette as a hybridization probe, the EcoRI digested DNA gave bands of 3.4 and 11.5 kb (Fig. 1 *B*; lanes *7* and *8*) indicating that homologous recombination of both arms of AMOGtk had occurred. The single band of 2.9 kb observed in the BamHI digested DNA using the neo probe (Fig. 1 *B*; lanes *5* and *6*) verified the absence of non-homologous recombination events. All seven recombinants identified by PCR showed only one homologous recombination event.

Three AMOG/β2 targeted embryonic stem cell clones were injected into C57BL/6J blastocysts and all clones gave germline transmitting male chimeras with a high degree of chimerism. Heterozygous mice showed no obvious abnormal behavioral phenotype. Approximately 25% of the offspring (N = 52) from crosses between heterozygous mice were homozygous for the mutation as identified by Southern blot analysis (Fig. 1 *B*; lanes 9–11), indicating that AMOG$^{(0/0)}$ mice did not die during embryonic development.

To confirm the generation of a null allele, we analyzed proteins from brains of AMOG$^{(0/0)}$ or AMOG$^{(+/+)}$ mice by immunoblotting (Fig. 1 *C*). Using either polyclonal or different monoclonal antibodies, no AMOG/β2 protein could be detected in crude membrane preparations of brains of AMOG$^{(0/0)}$ mice (Fig. 1 *C*; lane *3*, for monoclonal antibody 614), whereas AMOG/β2 was easily detected in AMOG$^{(+/+)}$ mice (Fig. 1 *C*, lane *2*) even at 100-fold less protein concentration (not shown). Immunocytochemical analysis of sections from different regions of the central nervous system of AMOG$^{(0/0)}$ mice using the two monoclonal AMOGβ2 antibodies 614 and 426 showed no immunoreactivity in comparison to AMOG$^{(+/+)}$ mice (Fig. 2 *e*, and not shown). In addition, in situ hybridization experiments were performed on tissue sections from AMOG$^{(+/+)}$ and AMOG$^{(0/0)}$ mice using an AMOG/β2 specific cRNA probe hybridizing with the region of the first exon of AMOG/β2 located upstream of the

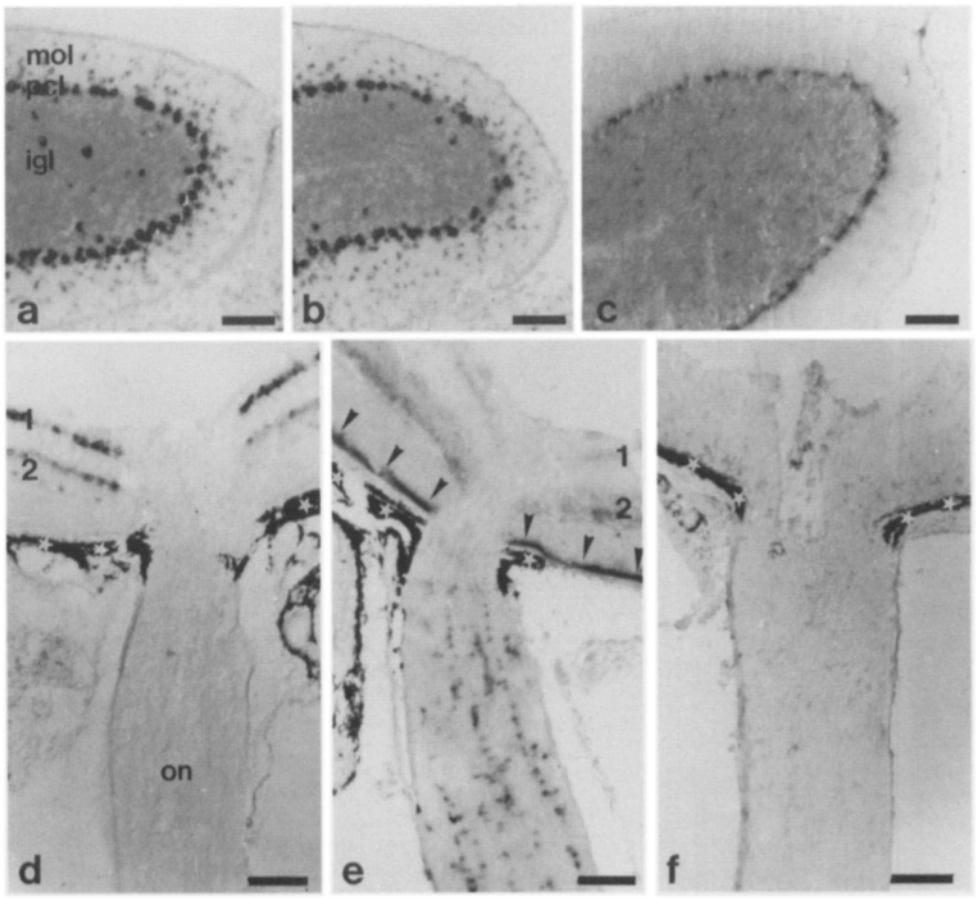

Figure 3. In situ hybridization analysis of the localization of AMOG/β2 (*c*, *e*, and *f*) and β1 (*a*, *b*, and *d*) mRNA in the cerebellar cortex (*a–c*) and retina and optic nerve (*d–f*) of 17-d-old AMOG$^{(+/+)}$ (*a*, *c–e*) and AMOG$^{(0/0)}$ (*b* and *f*) littermates. In the cerebellar cortex of AMOG$^{(+/+)}$ (*a*) and AMOG$^{(0/0)}$ (*b*) animals, β1 mRNA is present in Golgi and granule cells of the internal granular layer (*igl*), large-sized Purkinje cells of the Purkinje cell layer (*pcl*), and stellate and basket cells of the molecular layer (*mol*). AMOG/β2 mRNA is detectable in granule cells and astrocytes located in the internal granular layer and small-sized Bergmann glial cell bodies located in the region of the Purkinje cell layer (*c*). β1 mRNA is not visible in the optic nerve (*on*), but is present in retinal ganglion cells (*1*) and cells located in the inner nuclear layer (*2*; *d*). AMOG/β2 mRNA is weakly expressed by retinal ganglion cells and cells of the inner nuclear layer and strongly by photoreceptor cells (*arrowheads in e*). In the optic nerve, AMOG/β2 is present in glial cells located throughout the nerve (*e*). Using the AMOG/β2 cRNA anti-sense probe, no hybridization signal was detectable in the optic nerve or retina of AMOG$^{(0/0)}$ mice (*f*). The pigment epithelium is labeled by white asterisks. Bars: (*a–f*) 100 μm.

introduced mutation. No signal was detectable in sections from AMOG$^{(0/0)}$ (Fig. 3 *f*) animals whereas strong labeling was visible in sections of AMOG$^{(+/+)}$ (Fig. 3, *c* and *e*) mice.

Behavioral Phenotype of AMOG$^{(0/0)}$ Mice

No overt behavioral phenotype could be observed until the mice were 15-d-old. At this time, AMOG$^{(0/0)}$ mice showed reduced righting behavior and orientation when lifted by the tail and dropped gently into the cage. While wild-type or heterozygous mice landed on their feet and immediately moved around, AMOG$^{(0/0)}$ mice fell onto their side and paused for a few seconds before they stood up on their feet and started moving. This motor incoordination rapidly worsened within a few days. AMOG$^{(0/0)}$ mice appeared to develop paralysis in their forelimbs and were unable to hold their heads in a normal position. The hind limbs started to become tremorous and animals were no longer able to remain in an upright position. AMOG/β2 deficient mice opened their eyes at the correct age, but most of them kept them closed when the abnormal behavior became apparent. Mutant animals lying on their side still showed normal grasping reflexes and responded to sound. AMOG$^{(0/0)}$ mice died at postnatal days 17 or 18, 2–3-d after the first appearance of the subtle abnormal behavioral phenotype. However, as the motor incoordination increased, animals were no longer able to feed and drink. Efforts to keep the animals viable by artificial feeding failed.

Na,K-ATPase Activity

The Na,K-ATPase pump activity was determined in homogenates of brains of 16–17-d-old animals. Na,K-ATPase activities were not significantly different between AMOG$^{(0/0)}$ mice (1.67 ± 0.19 μmol/mg/h; $n = 4$) and wild-type mice (1.64 ± 0.17 μmol/mg/h; $n = 4$) ($p = 0.83$; according to Student's unpaired two-tailed t test).

Expression of the β Subunits of Na,K-ATPase

To characterize the expression of the β subunits at the protein level, we performed Western blot analysis of crude brain membrane preparations of 17–18-d-old homozygous AMOG-deficient, heterozygous, and wild-type mice (Fig. 1 *C*). Different mono- and polyclonal AMOG antibodies revealed that wild-type (Fig. 1 *C*; lane *2*) and heterozygous (not shown) mice expressed AMOG at similar levels. In contrast, AMOG/β2 was not detectable in AMOG$^{(0/0)}$ mice (Fig. 1 *C*; lane *3*). Expression levels of the β1 subunit were identical in AMOG$^{(0/0)}$ and AMOG$^{(+/+)}$ littermates (Fig. 1 *C*, lanes *4* and *5*).

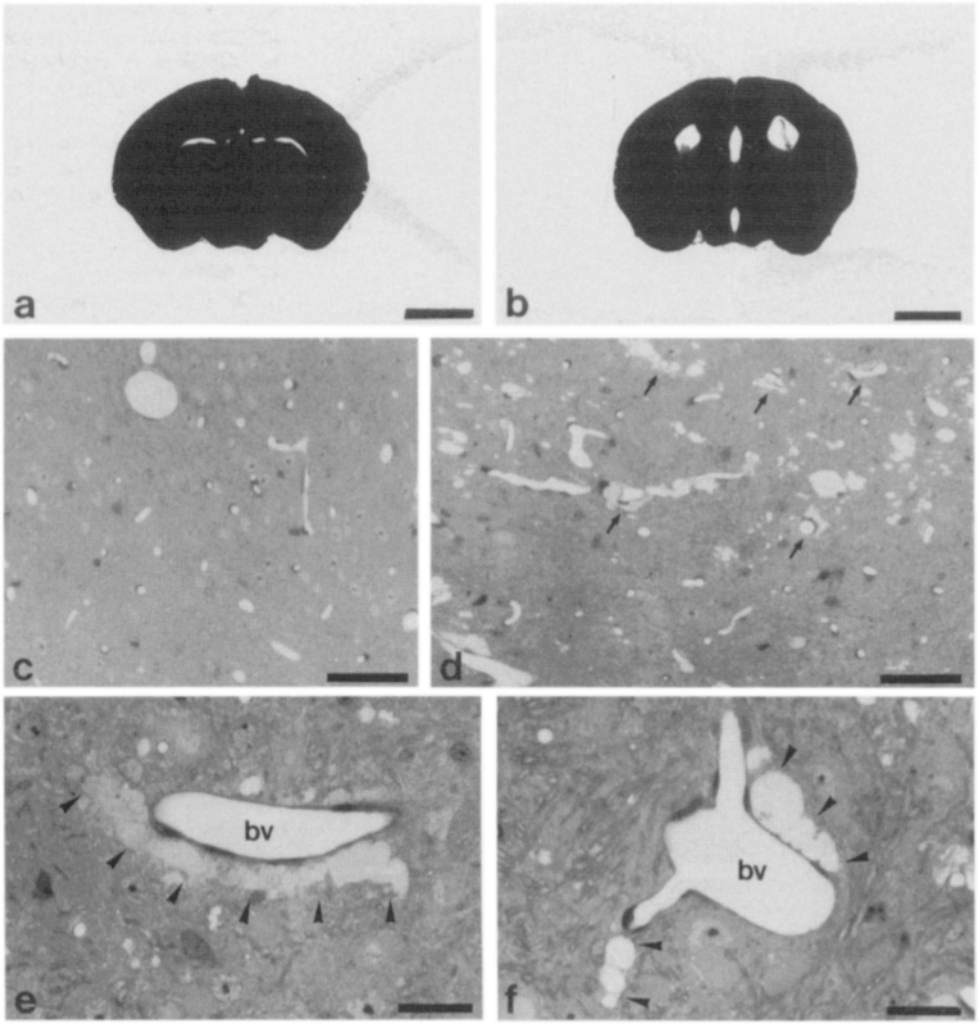

Figure 4. Light microscopic analysis of the ventricles (*a* and *b*) and brainstem (*c–f*) of AMOG$^{(0/0)}$ (*b*, *d–f*) and AMOG$^{(+/+)}$ (*a* and *c*) littermates. The lateral ventricles and the third ventricle of AMOG$^{(0/0)}$ mice (*b*) are significantly enlarged when compared to AMOG$^{(+/+)}$ littermates (*a*). In the brainstem of AMOG$^{(0/0)}$ (*d–f*) mice, swollen cellular structures (*d*, *arrowheads in e*) or vacuoles (*d*, *arrowheads in f*) are visible, usually in close association with blood vessels (*bv*; *arrows in d*). These morphological abnormalities were not detectable in corresponding regions of the brainstem of AMOG$^{(+/+)}$ animals (*c*). Bars: (*a* and *b*) 2.5 mm; (*c* and *d*) 50 μm; (*e* and *f*) 20 μm.

Expression of the Recognition Molecules N-CAM, L1, and MAG

The expression levels of N-CAM, L1, or MAG were similar in AMOG$^{(0/0)}$, AMOG$^{(+/0)}$ (not shown), and AMOG$^{(+/+)}$ littermates as determined by Western blot analysis of crude membrane preparations of 17–18-d-old brains (Fig. 1 *C*; lanes *7–12*).

Analysis of AMOG$^{(0/0)}$ Mice by Light and Electron Microscopy, Immunocytochemistry, and In Situ Hybridization

At the light microscope level, the lateral and third ventricles of AMOG$^{(0/0)}$ mice (Fig. 4 *b*) were significantly enlarged when compared to wild-type (Fig. 4 *a*) or heterozygous (not shown) littermates.

In the brain stem of AMOG$^{(0/0)}$ mice, swollen cellular processes and vacuoles were detectable, usually closely associated with blood vessels (Fig. 4, *d–f*). Swollen cellular processes and vacuoles were not detectable in corresponding regions of the brain stem of wild-type (Fig. 4 *c*) or heterozygous (not shown) littermates. For a more detailed analysis, brain stems of AMOG mutants were studied at the ultrastructural level. Confirming the light microscopic observations, swollen cellular processes (Fig. 5, *a* and *c*) and electron-lucent vacuoles (Fig. 5, *b* and *c*) were found in direct association with blood vessels. The close association between degenerating cellular processes and blood vessels suggests that degenerating cells represent astrocytes. The electron-lucent vacuoles thus most likely result from swelling and subsequent degeneration of astrocytic processes. Similar vacuolated structures were visible in the thalamus, striatum, and spinal cord (not shown).

Cerebellum. The cytoarchitecture of the cerebellar cortex of AMOG$^{(0/0)}$ (Fig. 6 *b*) mice appeared normal and the thickness of different cortical layers were similar to that of AMOG$^{(+/+)}$ (Fig. 6 *a*) littermates. In particular, the thickness of the internal and external granular layers of AMOG$^{(0/0)}$ animals and AMOG$^{(+/+)}$ littermates were similar, indicating that granule cell migration is not disturbed in the absence of AMOG/β2. In contrast to the brain stem, blood vessels of the cerebellar cortex were not associated with degenerating cellular elements. However, some degenerating Purkinje cells and some small-sized degenerating cells in the internal granular layer were present in AMOG$^{(0/0)}$ mice (not shown). In AMOG$^{(+/+)}$ mice, AMOG/β2 immunoreactivity was detectable in all cortical layers of the cerebellum (Fig. 2 *a*). Strong immunoreactivity was found in the internal granular layer. The molecular layer was homogeneously labeled, suggesting that the cell surfaces of parallel fibers are im-

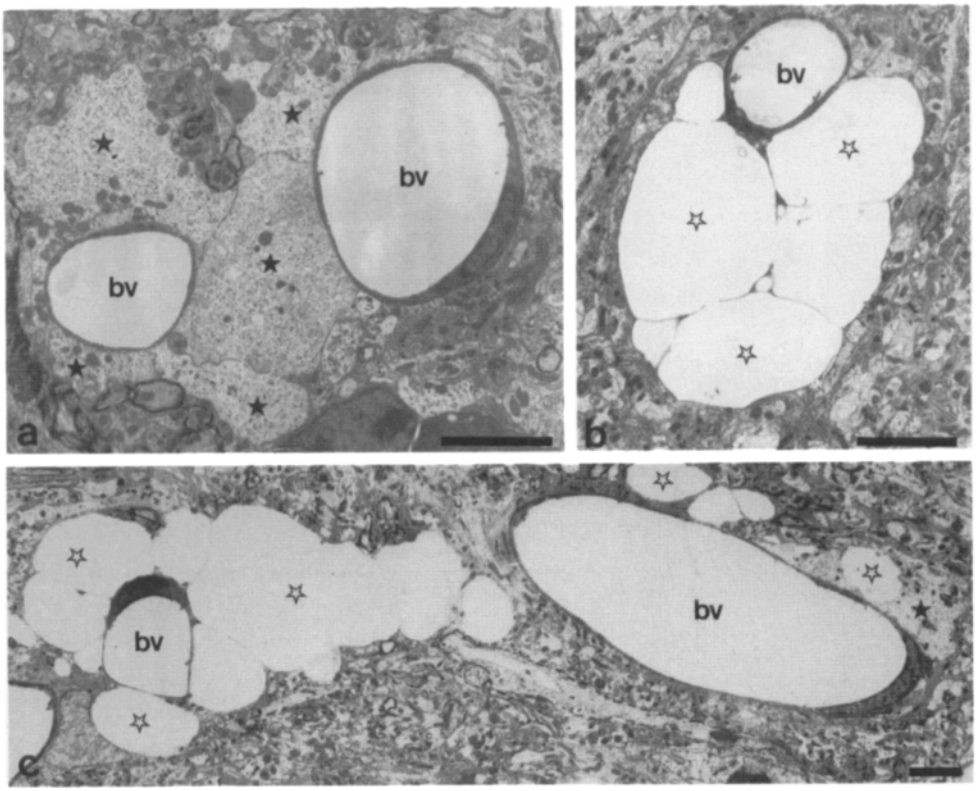

Figure 5. Electron microscopic analysis of the brainstem of 18-d-old AMOG$^{(0/0)}$ mice. Some blood vessels (*bv*) are surrounded by swollen and electron-lucent cellular processes (*filled asterisks in a and c*). In addition, blood vessels are also associated with electron-lucent intracellular vacuoles (*open asterisks in b and c*). Bars: (*a–c*) 4 μm.

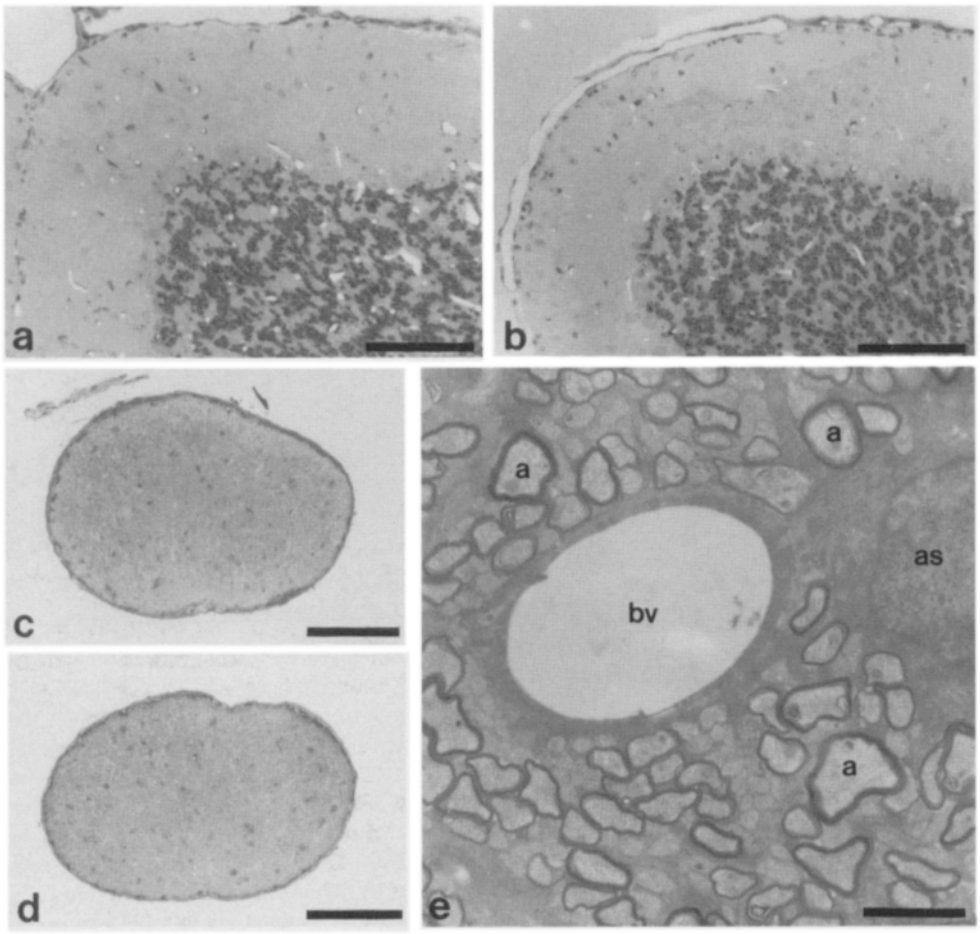

Figure 6. Histological analysis of the cerebellar cortex (*a* and *b*) and optic nerve (*c–e*) of 17-d-old AMOG$^{(+/+)}$ (*a* and *c*) and AMOG$^{(0/0)}$ (*b*, *d*, and *e*) littermates. The cerebellar cortex of AMOG$^{(+/+)}$ (*a*) and AMOG$^{(0/0)}$ (*b*) animals shows a similar cytoarchitecture, with a comparable thickness of the different cortical layer. The external granular layer of both animals has almost disappeared at this developmental age. Similarly, the optic nerve of AMOG$^{(0/0)}$ animals (*d*) shows no morphological abnormalities when compared with AMOG$^{(+/+)}$ littermates (*c*). Ultrastructurally, myelinated retinal ganglion cell axons (*a*) and astrocytes (*as*) and their processes abutting optic nerve blood vessels (*bv*) appear morphologically unaffected in AMOG$^{(0/0)}$ animals (*e*). Bars: (*a–d*) 100 μm; (*e*) 2 μm.

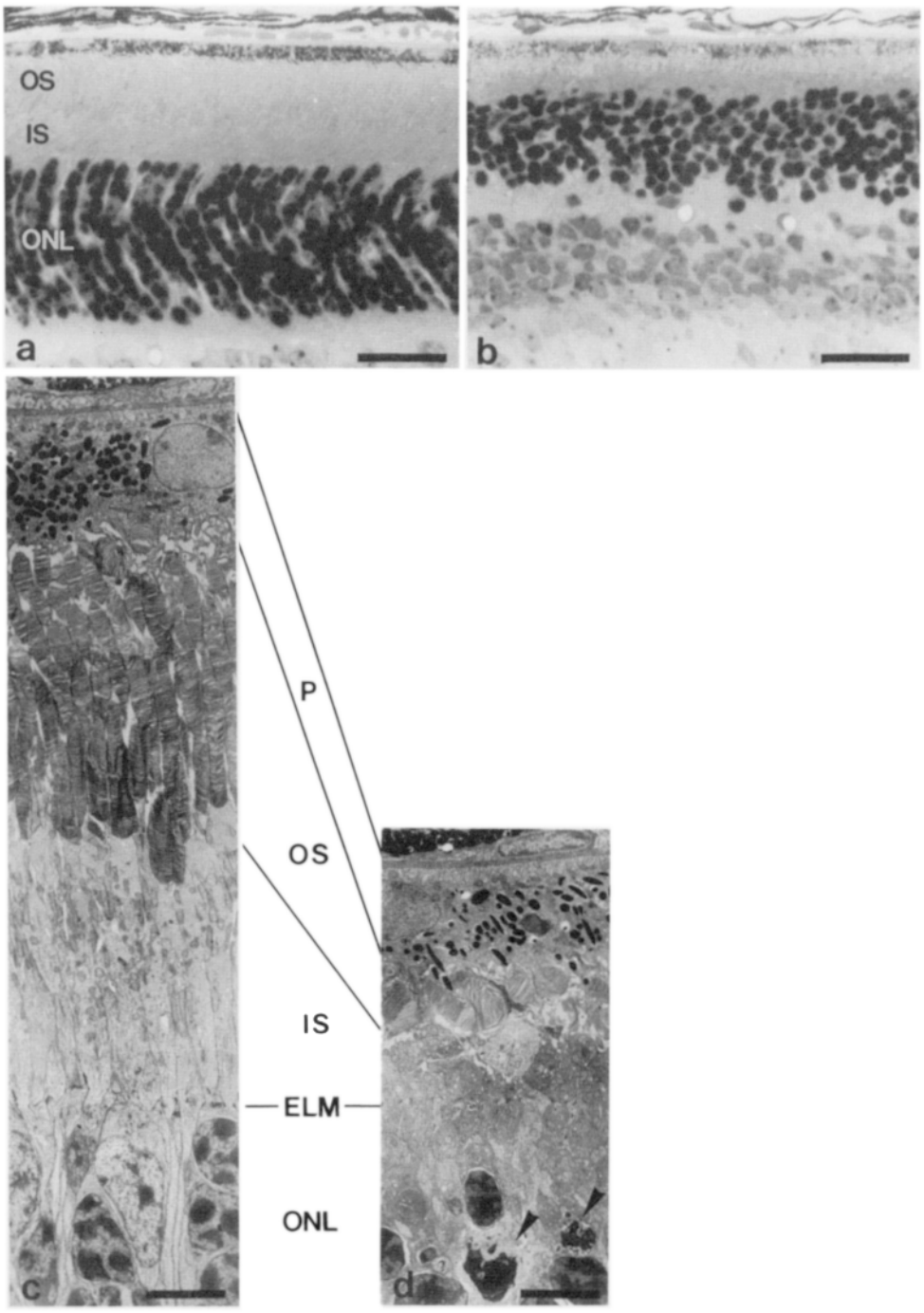

Figure 7. Light and electron microscopic analysis of photoreceptor cells of 17-d-old AMOG$^{(+/+)}$ (*a* and *c*) and AMOG$^{(0/0)}$ (*b* and *d*) littermates. The length of inner (*IS*) and outer (*OS*) segments of photoreceptor cells in AMOG$^{(0/0)}$ animals (*b* and *d*) is significantly reduced when compared to AMOG$^{(+/+)}$ littermates (*a* and *c*). Moreover, the outer nuclear layer (*ONL*) of AMOG$^{(0/0)}$ (*b*) mice is significantly reduced in thickness (*compare a and b*). Ultrastructurally, degenerating photoreceptor cells (*arrowheads in d*) are present in the outer nuclear layer of AMOG$^{(0/0)}$ mice. *P*, pigment epithelium; *ELM*, external limiting membrane. Bars: (*a* and *b*) 25 μm; (*c* and *d*) 5 μm.

munoreactive (Fig. 2 *a*). In situ hybridization analysis showed AMOG/β2 transcripts in cells located in the white matter (not shown). The internal granular layer was homogeneously labeled with the AMOG/β2 cRNA probe (Fig. 3 *c*), indicating that granule cells synthesize the molecule. Some cells, scattered throughout the internal granular layer, showed an increased labeling intensity. The number and distribution of these intensely labeled cells suggest that they correspond to astrocytes. AMOG/β2 mRNA was also detectable in the region of the Purkinje cell layer (Fig. 3 *c*). An analysis of these sections at higher magnification or of sections counterstained with methylene blue (not shown) revealed that the labeled cells corresponded to Bergmann glial cells. Purkinje cells, in contrast, contained no detectable levels of AMOG/β2 mRNA and no AMOG/β2 transcripts were detectable in the molecular layer (Fig. 3 *c*). β1 immunoreactivity was homogenously distributed in the molecular layer and internal granular layer of AMOG$^{(+/+)}$ (Fig. 2 *f*) and AMOG$^{(0/0)}$ (Fig. 2 *g*) animals. No differences in the intensity of immunolabeling were detectable (compare Fig. 2, *f* and *g*). Cells containing β1 mRNA were visible in the internal granular layer, Purkinje cell layer, and molecular layer (Fig. 3, *a* and *b*). As judged from the position and size of the cell bodies, β1-positive cells corresponded to granule and Golgi cells in the internal granular layer, Purkinje cells in the Purkinje cell layer, and stellate and basket cells in the

molecular layer. The intensity of the hybridization signal was similar in AMOG$^{(+/+)}$ and AMOG$^{(0/0)}$ animals (compare Fig. 3, *a* and *b*).

Optic nerve. Light microscopic analysis of optic nerves of AMOG$^{(0/0)}$ (Fig. 6 *d*) mice revealed no detectable histological changes in comparison to AMOG$^{(+/+)}$ (Fig. 6 *c*) littermates. No signs of degeneration were visible in the vicinity of blood vessels (Fig. 6, *d* and *e*). Compacted myelin, retinal ganglion cell axons, and astrocytic endfeet abutting onto blood vessels (Fig. 6 *e*) or forming the glial limiting membrane at the outer surface of the nerve (not shown) appeared ultrastructurally normal in AMOG$^{(0/0)}$ mice. In AMOG$^{(+/+)}$ mice, strong AMOG/β2-immunoreactivity was found in the distal myelinated part of the optic nerve (Fig. 2 *c*). In the proximal unmyelinated part of the nerve, AMOG/β2-immunoreactivity was homogeneously distributed (not shown), suggesting that along with optic nerve glial cells, retinal ganglion cell axons are AMOG/β-positive. By in situ hybridization, a subpopulation of glial cells was labeled by the AMOG/β2 cRNA probe in AMOG$^{(+/+)}$ animals (Fig. 3 *e*). Since labeled cells were not restricted to the myelinated distal part, but were also detectable in the unmyelinated retinal end of the optic nerve, these cells most likely represent astrocytes. Sections from AMOG$^{(0/0)}$ animals incubated with AMOG/β2 antibodies (Fig. 2 *e*) showed a weak background labeling, similar to that of AMOG$^{(+/+)}$ mice incubated with secondary antibodies only (Fig. 2 *d*). Similarly, sections from AMOG$^{(0/0)}$ mice hybridized with the AMOG/β2 anti-sense cRNA probe (Fig. 3 *f*) showed only weak background labeling comparable to that of AMOG$^{(+/+)}$ animals hybridized with the AMOG/β2 sense cRNA probe (not shown). Hybridization with the β1 cRNA probe showed no signal in the optic nerve (Fig. 3 *d*).

Retina. In AMOG$^{(0/0)}$ mice, the outer nuclear layer appeared to be reduced in thickness and contained numerous degenerating cells (Fig. 7 *b*). Moreover, the lengths of inner and outer segments of photoreceptor cells (Fig. 7, *b* and *d*) were significantly reduced when compared to that of AMOG$^{(+/+)}$ littermates (Fig. 7, *a* and *c*). Furthermore, degenerating photoreceptor cell bodies were observed at the ultrastructural level (Fig. 7 *d*). In contrast to the brain stem, retinal blood vessels were not associated with degenerating cellular elements. In the retinae of AMOG$^{(+/+)}$ animals, the nuclear layers, plexiform layers, and the nerve fiber layer were AMOG/β2-immunoreactive (Fig. 2 *b*). Strongest immunoreactivity was visible in association with the inner segments of photoreceptor cells (Fig. 2 *b*). AMOG/β2 transcripts were found in retinal ganglion cells, cells of the inner nuclear layer, and in photoreceptor cells (Fig. 3 *e*). β1 mRNA was detectable in retinal ganglion cells and a subpopulation of cells located in the inner nuclear layer, but not in photoreceptor cells (Fig. 3 *d*).

Discussion

We have generated mice deficient for the adhesion molecule on glia (AMOG/β2 subunit of Na,K-ATPase) by targeted disruption of its gene in embryonic stem cells. The position of the AMOG$^{(0/0)}$ mutation within the first exon generates a null allele as verified by immunochemical, immunocytochemical, and in situ hybridization experiments. AMOG$^{(0/0)}$ mice exhibit a characteristic behavioral phenotype that becomes apparent at postnatal day 15 by abnormalities in motor coordination, tremors, and paralysis with extremely rapid progression of symptoms leading to death at days 17–18. Mice heterozygous for the mutation appear unaffected.

In view of the abnormal phenotype of the mutant, it is worthwhile to review the expression of AMOG/β2 as a function of developmental stage and cell type in AMOG$^{(+/+)}$ mice. AMOG/β2 is hardly detectable outside the central nervous system (Antonicek et al., 1987; Antonicek and Schachner, 1988; Gloor et al., 1990; Martin-Vasallo et al., 1989; Pagliusi et al., 1990). The molecule is mainly expressed by glial cells, although expression by certain types of neurons could never be rigorously excluded and has, in fact, recently been demonstrated (Antonicek et al., 1987; Pagliusi et al., 1990; Schneider et al., 1991; this study). Its expression is first detectable in the brain at late fetal stages, increases during the first two postnatal weeks, and reaches highest levels in the adult (Pagliusi et al., 1990).

Histological analysis of AMOG$^{(0/0)}$ mice shortly after the onset of behavioral abnormalities reveals that several brain regions display a normal histological phenotype at the light microscopic level. For example, the cytoarchitecture of the cerebellar and cerebral cortices and hippocampus (unpublished observations) appears to be normal. The question thus arises whether AMOG/β2 plays a profound morphogenetic role during formation of these brain regions. In difference to the apparently normal differentiation of the cerebellar cortex of AMOG$^{(0/0)}$ mice, AMOG/β2 antibodies have been demonstrated to interfere with granule cell migration in vitro (Antonicek et al., 1987). This discrepancy might result from the fact that other recognition molecules known to be functionally involved in migration of granule cells, such as the neural recognition molecules tenascin (Chuong et al., 1987; Husmann et al., 1992), thrombospondin (O'Shea et al., 1990), L1 (Lindner et al., 1983), and possibly others, are able to compensate for the lack of AMOG/β2 expression in the mutant. It is noteworthy in this respect that the expression of the recognition molecules L1, N-CAM, and myelin-associated glycoprotein was found to be normal in the AMOG mutant. To resolve whether AMOG/β2 plays a subtle role in morphogenetic cell interactions, the differentiation, and, in particular, the migration of granule cells will have to be analyzed systematically in a developmental time sequence.

We suggest that the abnormal histological phenotype observed in some brain regions of the mutant can be explained on the basis of altered Na^+ pump activity, as AMOG/β2 is an integral component of the Na,K-ATPase. For instance, degeneration of some neural cells in the AMOG mutant could be due to the failure of pump activity, being in particular demand in highly active cells, such as the photoreceptor cells, the primary sensory neurons of the retina. The swelling and consecutive disintegration of astrocytic endfeet, particularly near capillaries, is another indication of the failure in pump activity at locations requiring tight regulation of ionic homeostasis. The resulting osmoregulatory imbalance may lead to spongiform encephalopathy which is characterized by intracellular vacuoles in the brain tissue as observed in other neurodegenerative disorders of various etiologies (Eisiri and Kennedy, 1992; Kamin and Petito, 1991; Prusiner, 1991). Attempts to directly relate the histological

phenotype of the AMOG/β2 deficient mice to a decreased pump activity failed, since we did not detect a significant decrease of Na,K-ATPase activity in tissue homogenates of brains of AMOG-deficient mice. This finding may result from the fact that tissue from the entire brain was used for this analysis. However, only circumscribed small areas of the brain are morphologically affected in the mutant. Furthermore, although exact values of Na,K-ATPase activity are available that relate to the relative abundance of the individual α subunits in the brain at the protein level, Northern blot analysis and our own in situ hybridization experiments (Molthagen, M., and U. Bartsch, unpublished observations) show that at the mRNA level, the α3 subunit is the most abundant α subunit in differentiated rodent brain tissue. Since the α3 subunit predominantly associates with β1, it is likely that a possible decrease in ATPase activity contributed by the complex between AMOG/β2 and α2 would not have been detectable due to the relative abundance of the complex between β1 and α3. The present observations, therefore, do not yield conclusive interpretations as to the correlation between pump activity and morphologically detectable degeneration of neural cell types.

The spongiform status of the AMOG/β2 mutant is confined to the brain stem, thalamus and striatum, and, to a lesser degree, to the spinal cord, but is not observed in cerebellum and hippocampus, where AMOG/β2 is most prominently expressed (Pagliusi et al., 1990). It is presently not known why some brain regions show spongiform abnormalities while others do not. However, it is conceivable that compensatory mechanisms at the individual cell level have to be considered. This possibility is supported by the observation that only some, but not all cells that express AMOG/β2 in the wild-type degenerate in the mutant. The two β subunits presently known are both able to interact with more than one α subunit to yield a fully functional Na^+ pump (Schmalzing et al., 1992). It is therefore possible that the few cells expressing both β subunits, such as the cerebellar granule cells or retinal ganglion cells, are able to survive in the AMOG/β2 mutant, because the β1 subunit may take over at least some of the functions of AMOG/β2. However, some cell types, such as glial cells in the optic nerve, express only AMOG/β2 in the wild-type animal but are also unaffected in the mutant. These cells may express a yet unidentified β subunit and thus a functionally active Na^+ pump. Alternatively, the β1 subunit may be present in these cell types at earlier developmental ages and might then be substituted by AMOG/β2 during the third postnatal week. Evidence for a developmental switch in the expression of the β subunits, i.e., downregulation of the β1 subunit and concomitant upregulation of AMOG/β2 in several neural cell types has recently been obtained (Molthagen, M., and U. Bartsch, unpublished observations). According to these observations, the time of degeneration of cells in the AMOG/β2 mutant may correspond to the time of the switch in expression of β subunits: neural cell types in which AMOG/β2 substitutes β1 early during development are morphologically affected, whereas cells in which AMOG/β2 substitutes β1 late in development appear morphologically unaffected at the time of the mutant's death.

A failure in the ionic homeostasis similar to that of the AMOG/β2 mutant has been observed in the *mec-4* mutant of *Caenorhabditis elegans* (Driscoll and Chalfie, 1991). The *mec-4* gene product is related to the Na^+ channel of intestinal epithelia in mammals (Canessa et al., 1993). Neurons in the *mec-4* mutant swell and reach several times their normal diameter before degeneration. The cellular defects of the *mec-4* mutation are probably due to an impaired regulation of the ion channel resulting in an enhanced entry of Na^+ and water into the cell. These observations are in agreement with our interpretation of the abnormal phenotype of the AMOG/β2 mutant.

Finally, the question remains as to the cause of the mutant's death. We can presently not exclude that other organs in which AMOG/β2 is negligibly expressed may be involved. However, we presently consider it more likely that the animal's death is due to the dysfunction of vitally important brain structures, such as the brain stem and spinal cord. Morphological analysis of other organs and physiological analysis of the cellular functions of neurons and glia in vitro and in vivo should clarify these questions.

We are grateful to Dr. Karl Peter Giese for excellent assistance in gene-targeting experiments, E. Gui-Xia Yu for technical assistance, Drs. Gerhild Müller, Sergio Gloor, Philip Beesley (University of London), Kathleen J. Sweadner (Harvard Medical School), and Carolin Schmidt for providing antibodies, Dr. Michel Aguet (University of Zurich) for many helpful discussions, and Dr. D. Montag and M. Molthagen for critically reading the manuscript.

This work was supported by Schweizerischer Nationalfond.

Received for publication 23 June 1994 and in revised form 20 July 1994.

References

Antonicek, H. V., and M. Schachner. 1988. The adhesion molecule on glia (AMOG) incorporated into lipid vesicles binds to subpopulations of neurons. *J. Neurosci.* 8:2961–2966.

Antonicek, H., E. Persohn, and M. Schachner. 1987. Biochemical and functional characterization of a novel neuron-glia adhesion molecule that is involved in neuronal migration. *J. Cell Biol.* 104:1587–1595.

Bartsch, U., F. Kirchhoff, and M. Schachner. 1989. Immunohistological localization of the adhesion molecules L1, N-CAM, and MAG in the developing and adult optic nerve of mice. *J. Comp. Neurol.* 284:451–462.

Bartsch, S., U. Bartsch, U. Dörries, A. Faissner, A. Weller, P. Ekblom, and M. Schachner. 1992*a*. Expression of tenascin in the developing and adult cerebellar cortex. *J. Neurosci.* 12:736–749.

Bartsch, U., S. Bartsch, U. Dörries, and M. Schachner. 1992*b*. Immunohistological localization of tenascin in the developing and lesioned adult mouse optic nerve. *Eur. J. Neurosci.* 4:338–352.

Beesley, P. W., T. Paladino, C. Gravel, R. A. Hawkes, and J. W. Gurd. 1987. Characterization of gp 50, a major glycoprotein present in rat brain synaptic membranes, with a monoclonal antibody. *Brain Res.* 408:65–78.

Bollensen, E., and M. Schachner. 1987. The peripheral myelin glycoprotein P0 expresses the L2/HNK-1 and L3 carbohydrate structures shared by neural adhesion molecules. *Neurosci. Lett.* 82:77–82.

Bradford, M. M. 1976. A rapid and sensitive method for quantitation of microgram quantities of protein utilizing the principle of protein-dye binding. *Anal. Biochem.* 72:248–254.

Canessa, C. M., J.-D. Horisberger, and B. C. Rossier. 1993. Epithelial sodium channel related to proteins involved in neurodegeneration. *Nature (Lond.).* 361:467–470.

Chuong, C.-M. K. L. Crossin, and G. M. Edelman. 1987. Sequential expression and differential function of multiple adhesion molecules during the formation of cerebellar cortical layers. *J. Cell Biol.* 104:331–342.

Doetschman, T. C., H. Eistetter, M. Katz, W. Schmidt, and R. Kemler. 1985. The *in vitro* development of blastocyst-derived embryonic stem cell lines: formation of visceral yolk sac, blood islands and myocardium. *J. Embryol. Exp. Morphol.* 87:27–45.

Dörries, U., U. Bartsch, C. Nolte, J. Roth, and M. Schachner. 1993. Adaptation of a non-radioactive in situ hybridization method to electron microscopy: detection of tenascin mRNAs in mouse cerebellum with digoxigenin-labelled probes and gold-labelled antibodies. *Histochemistry.* 99:251–262.

Driscoll, M. V., and M. Chalfie. 1991. The *mec-4* gene is a member of a family of *Caenorhabditis elegans* genes that can mutate to induce neuronal degeneration. *Nature (Lond.).* 349:588–593.

Eisiri, M. M., and P. G. E. Kennedy. 1992. Virus diseases. Greenfield's Neuropathology. 335–399. A. J. Hume and L. W. Duchen, editors. Edward Arnold, London. 557 pp.

Fahrig, T., B. Schmitz, D. Weber, A. Kücherer-Ehret, A. Faissner, and M. Schachner. 1990. Two monoclonal antibodies recognizing carbohydrate epitopes on neural adhesion molecules interfere with cell interactions. *Eur. J. Neurosci.* 2:153–161.

Giese, K. P., R. Martini, G. Lemke, P. Soriano, and M. Schachner. 1992. Mouse Po gene disruption leads to hypomyelination, abnormal expression of recognition molecules, and degeneration of myelin and axons. *Cell.* 71: 565–576.

Gloor, S. 1989. Cloning and nucleotide sequence of the mouse Na,K-ATPase β subunit. *Nucleic Acids Res.* 17:10117.

Gloor, S., H. Antonicek, K. J. Sweadner, S. Pagliusi, R. Frank, M. Moos, and M. Schachner. 1990. The adhesion molecule on glia (AMOG) is a homolog of the β subunit of the Na,K-ATPase. *J. Cell Biol.* 110:165–174.

Gorvel, G. P., A. Liabeuf, D. Massey, D. Liot, C. Goridis, and S. Maroux. 1984. (Na^+ + K^+)-ATPase recognition in mouse organs by a monoclonal antibody. *Cell Tissue Res.* 238:253–261.

Hasty, P., J. Rivera-Perez, C. Chang, and A. Bradley. 1991. Target frequency and integration pattern for insertion and replacement vectors in embryonic stem cells. *Mol. Cell. Biol.* 11:4509–4517.

Hille, B. 1984. Ionic channels of excitable membranes. Sinauer, Sunderland, MA. 426 pp.

Hodgkin, A. L. 1964. The conduction of the nervous impulse. Liverpool University Press, Liverpool, UK.

Horstkorte, R., M. Schachner, J. P. Magyar, T. Vorherr, and B. Schmitz. 1993. The fourth immunoglobulin-like domain of NCAM contains a carbohydrate recognition domain for oligomannosidic glycans implicated in association with L1 and neurite outgrowth. *J. Cell Biol.* 121:1409–1421.

Husmann, K., A. Faissner, and M. Schachner. 1992. Tenascin promotes cerebellar granule cell migration and neurite outgrowth by different domains in the fibronectin type III repeats. *J. Cell Biol.* 116:1475–1486.

Kamin, S. S., and C. K. Petito. 1991. Idiopathic myelopathies with white matter vacuolation in non-acquired immunodeficiency syndrome patients. *Hum. Pathol.* 22:816–824.

Keilhauer, G., A. Faissner, and M. Schachner. 1985. Differential inhibition of neurone-neurone, neurone-astrocyte and astrocyte-astrocyte adhesion by L1, L2 and N-CAM antibodies. *Nature (Lond.).* 316:728–730.

Kimelberg, H. K. 1991. Swelling and volume control in brain astroglial cells. In Comparative and Environmental Physiology. Vol. 9. R. Gilles, E. K. Hoffmann, L. Bolis, editors. Springer, New York. pp 81–117.

Kogan, S. C., M. Doherty and J. Gitschier. 1987. An improved method for prenatal diagnosis of genetic diseases by analysis of amplified DNA sequences. *New Engl. J. Med.* 317:985–990.

Kücherer, A., A. Faissner, and M. Schachner. 1987. The novel carbohydrate epitope L3 is shared by some neural cell adhesion molecules. *J. Cell Biol.* 104:1597–1602.

Lindner, J., F. G. Rathjen, and M. Schachner. 1983. L1 mono- and polyclonal antibodies modify cell migration in early postnatal mouse cerebellum. *Nature (Lond.).* 305:427–430.

Magyar, J. P., and M. Schachner. 1990. Genomic structure of the adhesion molecule on glia (AMOG, Na/K-ATPase β2 subunit). *Nucleic Acids Res.* 18:6695–6696.

Mansour, S. L., K. R. Thomas, and M. R. Capecchi. 1988. Disruption of the protooncogene int-2 in mouse embryo-derived stem cells: a general strategy for targeting mutations to non-selectable genes. *Nature (Lond.).* 336:348–352.

Martin-Vasallo, P., W. Dackowski, J. R. Emanuel, and R. Levenson. 1989. Identification of a putative isoform of the Na,K-ATPase β subunit: primary structure and tissue-specific expression. *J. Biol. Chem.* 264:4613–4618.

Martini, R., and M. Schachner. 1986. Immunoelectron microscopic localization of neural cell adhesion molecules (L1, N-CAM, and MAG) and their shared carbohydrate epitope and myelin basic protein in developing sciatic nerve. *J. Cell Biol.* 103:2439–2448.

Müller-Husmann, G., S. Gloor, and M. Schachner. 1993. Functional characterisation of β isoforms of murine Na,K-ATPase: the adhesion molecule on glia (AMOG/β2), but not β1, promotes neurite outgrowth. *J. Biol. Chem.* 268:26260–26267.

O'Shea, K. S., J. S. T. Rheinheimer, and V. M. Dixit. 1990. Deposition and role of thrombospondin in the histogenesis of the cerebellar cortex. *J. Cell Biol.* 110:1275–1283.

Pagliusi, S. R., M. Schachner, P. H. Seeburg, and B. D. Shivers. 1990. The adhesion molecule on glia (AMOG) is widely expressed by astrocytes in developing and adult mouse brain. *Eur. J. Neurosci.* 2:471–480.

Pesheva, P., A. F. Horwitz, and M. Schachner. 1987. Integrin, the cell surface receptor for fibronectin and laminin, expresses the L2/HNK-1 and L3 carbohydrate structure shared by adhesion molecules. *Neurosci. Lett.* 83: 303–306.

Poltorak, M., R. Sadoul, G. Keilhauer, C. Landa, T. Fahrig, and M. Schachner. 1987. Myelin-associated glycoprotein, a member of the L2/HNK-1 family of neural cell adhesion molecules, is involved in neuron-oligodendrocyte and oligodendrocyte-oligodendrocyte interaction. *J. Cell Biol.* 105:1893–1899.

Prusiner, S. B. 1991. Molecular biology of prion diseases. *Science (Wash. DC).* 252:1515–1522.

Rathjen, F. G., and M. Schachner. 1984. Immunocytological and biochemical characterization of a new neuronal cell surface component (L1 antigen) which is involved in cell adhesion. *EMBO (Eur. Mol. Biol. Organ.) J.* 3:1–10.

Schmalzing, G., S. Gloor, H. Omay, S. Kröner, H. Appelhans, and W. Schwarz. 1991. Up-regulation of sodium pump activity in *Xenopus laevis* oocytes by expression of heterologous β1 subunits of the sodium pump. *Biochem. J.* 279:329–336.

Schmalzing, G., S. Kröner, M. Schachner, and S. Gloor. 1992. The adhesion molecule on glia (AMOG/β2) and α1 subunits assemble to functional sodium pumps in Xenopus oocytes. *J. Biol. Chem.* 267:20212–20216.

Schmitz, B., J. Peter-Katalinic, H. Egge, and M. Schachner. 1993. Monoclonal antibodies raised against membrane glycoproteins from mouse brain recognize N-linked oligomannosidic glycans. *Glycobiology.* 3:609–617.

Schneider, B. G., A. W. Shyjan, and R. Levenson. 1991. Co-localization and polarized distribution of Na,K-ATPase α3 and β2 subunits in photoreceptor cells. *J. Histochem. Cytochem.* 39:507–517.

Shyjan, A. W., V. A. Canfield, and R. Levenson. 1991. Evolution of the Na,K- and H,K-ATPase β subunit gene family: structure of the murine Na,K-ATPase β2 subunit gene. *Genomics.* 11:435–442.

Soriano, P., C. Montgomery, R. Geske, and A. Bradley. 1991. Targeted disruption of the c-src proto-oncogene leads to osteopetrosis in mice. *Cell.* 64:693–702.

Wang, Z.-Q., A. E. Grigoriadis, U. Möhle-Steinlein, and E. F. Wagner. 1991. A novel target of c-fos-induced oncogenesis: development of chondrogenic tumours in embryonic stem cell chimeras. *EMBO (Eur. Mol. Biol. Organ.) J.* 10:2437–2450.